Computing the diffusivity of a particle subject to dry friction with colored noise

Josselin Garnier*
Centre de Mathématiques Appliquées, Ecole Polytechnique, Institut Polytechnique de Paris, 91120 Palaiseau, France

Laurent Mertz†
Department of Mathematics, City University of Hong Kong, Kowloon, Hong Kong, China

(Received 20 May 2023; accepted 25 September 2023; published 25 October 2023)

This paper considers the motion of an object subjected to a dry friction and an external random force. The objective is to characterize the role of the correlation time of the external random force. We develop efficient stochastic simulation methods for computing the diffusivity (the linear growth rate of the variance of the displacement) and other related quantities of interest when the external random force is white or colored. These methods are based on original representation formulas for the quantities of interest, which make it possible to build unbiased and consistent estimators. The numerical results obtained with these original methods are in perfect agreement with known closed-form formulas valid in the white-noise regime. In the colored-noise regime, the numerical results show that the predictions obtained from the white-noise approximation are reasonable for quantities such as the histograms of the stationary velocity but can be wrong for the diffusivity unless the correlation time is extremely small.

DOI: 10.1103/PhysRevE.108.045309

I. INTRODUCTION

The present work is motivated by the study of the motion of an object subjected to a dry friction and an external random force. The dry friction model in our paper is the standard model to study macroscopic systems involving solid-solid friction [1,2].

This dry friction model is rather well understood when the external random force is a white noise [3–5]. The probability distribution of functionals of the velocity or the position can then be studied in detail [6,7]. Different generalizations have been considered, such as the motion of a particle bound to a spring being pulled at a definite speed, moving on a surface with dry friction in a noisy environment [8]. Moreover, emerging applications are found for biological systems. The effects of diffusion on the dynamics of a single focal adhesion at the leading edge of a crawling cell are investigated in [9] by considering a simplified model of sliding friction. To understand the stick-slip dynamics of migrating cells on viscoelastic substrates, a theoretical model of the leading edge dynamics of crawling cells is introduced in [10].

In our paper we address the role of the correlation time of the external force when it is a colored noise. No explicit formula is available, and therefore the analysis goes through numerical simulations. Nonetheless, it should be pointed out that an approximate expression of the stationary probability density function of the velocity has been proposed in [11]. Our goal is to present appropriate stochastic algorithms to estimate the quantities of interest and to discuss the relationships between the quantities of interest such as the displacement mobility and diffusivity and the input parameters such as the noise strength and correlation time.

We consider the one-dimensional displacement U of an object (with unit mass) lying on a motionless surface. The velocity is denoted by V and thus $V = \dot{U}$, where the dot stands for time derivative throughout the paper. As shown schematically in Fig. 1, Newton's law of motion implies $\dot{V} + \mathbb{F} = f$, where $\mathbb{F}$ corresponds to the dry friction force and f represents all the other external and internal forces, including random perturbations. The force $\mathbb{F}$ cannot be expressed in terms of a standard function but as follows:

$$\mathbb{F} = \begin{cases} f, & \text{when } V = 0 \text{ and } |f| \leqslant \Delta, \\ \sigma\Delta, & \text{when } V \neq 0 \text{ or } (V = 0 \text{ and } |f| > \Delta), \end{cases}$$

where $\sigma = \mathrm{sgn}(V)$ when $V \neq 0$, otherwise $\sigma = \mathrm{sgn}(f)$. The coefficient $\Delta > 0$ is the coefficient of dry friction. The random perturbation induces a random displacement, and thus we can define the diffusivity of the displacement U as

$$D = \lim_{t\to+\infty} D^t \text{ where } D^t = \frac{\mathrm{var}(U(t))}{t}. \tag{1}$$

Such a friction model has been discussed by de Gennes [3]. When $f = \sqrt{\Gamma}\dot{W}$, where $\dot{W}$ is a white noise (i.e., the time derivative of Brownian motion W) and $\Gamma > 0$ is the noise strength, he formally proposed an expansion of the transition probability density of V in terms of eigenmodes related to a one-dimensional Schrödinger equation where the potential contains an attractive delta function. As a consequence, he obtained an approximate formula for the correlation function of the velocity. From this formula he suggested that the diffusivity scales as $D \sim \Gamma^3/\Delta^4$. A similar scaling was already proposed in a much earlier work by Caughey and Dienes

*josselin.garnier@polytechnique.edu
†lmertz@cityu.edu.hk

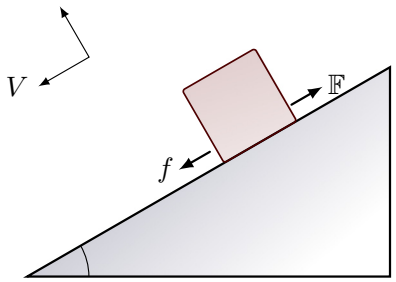

FIG. 1. Schematic of a solid object drifting downwards on a flat inclined support by overcoming the forces of dry friction $\mathbb{F}$.

[12]. The diffusivity is more sensitive to the noise power, in contrast to the case where dry friction is replaced by viscous friction, that is, $\Delta = 0$ and $f = -\tau_L^{-1} V + \sqrt{\Gamma}\dot{W}$ with $\tau_L > 0$ a relaxation time. Indeed, in this case $D = \tau_L^2 \Gamma$.

Touchette *et al.* [4,5] extended de Gennes' work and obtained without any approximation both the time-dependent transition probability density function and the correlation function of the velocity by solving the associated time-dependent Fokker-Planck equation. Touchette's results are exact when $f = \sqrt{\Gamma}\dot{W}$ or based on series representation when $f = -\tau_L^{-1} V + \sqrt{\Gamma}\dot{W}$, but they do not cover the case of colored noise. These results, however, will be important to us, because the stochastic simulation methods that we propose in our paper can be applied in particular to Touchette's configurations, and the results deduced from our simulations can, therefore, be tested against exact formulas for these configurations. Our simulation methods, however, can be applied to more general configurations and will unravel behaviors not covered by the previously known formulas.

Goohpattader *et al.* [13] have experimentally investigated physical friction problems that can be modeled using the aforementioned framework. They considered a forcing of the form $f = -\tau_L^{-1} V + \bar{\gamma} + \sqrt{\Gamma}\dot{W}$, where $\bar{\gamma}$ is a constant related to gravity and the inclination of the surface on which the system is installed. They also proposed numerical simulations. They observed experimentally and by simulation that the variance of the object displacement grows linearly with time, and they also observed scaling laws for the diffusivity that we will challenge in our paper.

Recently, some of the authors of the present paper have considered the case where $f = \mathfrak{b}(V) + \sqrt{\Gamma}X$, where $\mathfrak{b}(.)$ is a general function with appropriate conditions, and X is a pure jump noise (i.e., a piecewise constant random process). In [14] they proposed a piecewise deterministic Markov process (PDMP) to model the pair (X, V). This framework makes it possible to use the theory and simulation methods of PDMPs [15,16]. They derived the Kolmogorov equations for the pair (X, V). When $\mathfrak{b}(.)$ is an odd function, they showed ergodicity and provided a representation formula of the stationary state in terms of a portion of the trajectory called short excursion. Essentially, a short excursion contains only one dynamic phase, a time interval on which $V \neq 0$ or $|f| > \Delta$, and only one static phase, a time interval on which $V = 0$ and $|f| \leqslant \Delta$.

We develop our present article on the basis of the PDMP framework mentioned above and introduce new stopping times which identify independent components in the dynamics. These components are different from the short excursions. We call them *long excursions*. Having identified this type of trajectory portion we can express the diffusivity (or any related quantity) as an expectation of a functional of a long excursion, and we can, therefore, estimate these quantities by sampling long excursions directly, instead of sampling long-time period integrals on the original PDMP. We finally extend the notion of long excursion together with the corresponding sampling method to the limiting system case when the time step of the PDMP goes to zero. The latter is formulated using a differential inclusion [17,18] forced by a colored noise. The estimators based on our stochastic simulation methods are unbiased, contrarily to the standard estimation methods that consist in taking long but fixed-length trajectories. They are consistent and asymptotically normal. Their accuracies are sufficient to be used to discuss quantitative relations between the diffusivity and the noise strength and correlation time. In particular, they show that the predictions for the values of the diffusivity obtained from the white-noise approximation can be wrong when the correlation time of the noise is moderately small.

This paper is organized as follows: Section II proposes a dimensional analysis of the system in order to identify its effective parameters. Section III describes the PDMP framework modeling the friction problem and defines the original notion of long excursion. Section IV presents our characterization of the displacement diffusivity using long excursions. The resulting algorithm and an *ad hoc* Monte Carlo estimator are proposed in Sec. V. In Sec. VI, the notion of long excursion and the resulting numerical approach are extended from the PDMP case to the limiting differential inclusion case. Numerical simulations for the relation between the noise strength and correlation time and the diffusivity are studied in Sec. VII. Finally, we conclude in Sec. VIII.

II. EFFECTIVE PARAMETERS AND NONDIMENSIONAL SYSTEM

The driving noise with a correlation time $\tau > 0$ is represented by X, and the resulting velocity V satisfies, using the notation $f = \mathfrak{b}(V) + \sqrt{\Gamma}X$ with $\mathfrak{b}(v)$, a Lipschitz continuous function,

$$\begin{aligned} &\dot{V} = f - \sigma\Delta, && \text{when } V \neq 0 \text{ or } |f| > \Delta \text{ (dynamic phase)},\\ &\dot{V} = 0, && \text{when } V = 0 \text{ and } |f| \leqslant \Delta \text{ (static phase)}, \end{aligned} \tag{2}$$

where we have denoted $\sigma = \mathrm{sgn}(V)$ when $V \neq 0$, otherwise $\sigma = \mathrm{sgn}(f)$. Equation (2) can equivalently be written in the form of a multivalued stochastic differential equation (MSDE):

$$\dot{V} + \partial\varphi(V) \ni \mathfrak{b}(V) + \sqrt{\Gamma}X. \tag{3}$$

Here $\varphi(v) = \Delta|v|$, and its subdifferential $\partial\varphi$ is the set-valued map given by $\partial\varphi(0) = [-\Delta, \Delta]$ (interval) and $\partial\varphi(V) = \{\mathrm{sgn}(V)\Delta\}$ (singleton) when $V \neq 0$. The MSDE is a concise and rigorous way to formulate the transition between static and dynamic phases. A gentle introduction to MSDEs can be found in Chap. 4 of [17].

Below we derive the effective parameters and the corresponding nondimensional system. We remark that the physical parameters Δ and Γ are expressed in $\mathrm{m\,s^{-2}}$ and in

$m^2\,s^{-3}$, respectively. We can then introduce the reference time and space units $\tau_0 = \Gamma\Delta^{-2}$ (in s) and $u_0 = \Gamma^2\Delta^{-3}$ (in m). We deduce the nondimensional variables

$$t' = t/\tau_0, \quad V'(t') = V(t'\tau_0)\tau_0/u_0, \quad X'(t') = X(t'\tau_0)\tau_0^{1/2}. \tag{4}$$

When $\mathfrak{b}(v) = -v/\tau_L + \bar{\gamma}$, we can recast Eq. (3) into the nondimensional form

$$\dot{V}' + \partial|V'| \ni -V'/\tau_L' + \bar{\gamma}' + X', \tag{5}$$

where $\tau_L' = \tau_L/\tau_0$, $\bar{\gamma}' = \bar{\gamma}/(u_0/\tau_0^2) = \bar{\gamma}/\Delta$, and the dot stands for the derivative with respect to t'. Moreover, the effective noise correlation time from the nondimensional dynamics is $\tau' = \tau/\tau_0$. We will discuss the impact of τ' on the statistics of the system.

III. THE PDMP SYSTEM

In this section we present the system that describes the motion driven by a dry friction and an external random, stepwise constant force.

A. Description of the pure jump noise

We first define the driving colored noise X as a Markov jump process. Let $\delta > 0$ be a grid step (for the noise). The process X takes values in the finite state space $S^\delta = \delta\mathbb{Z} \cap [-L_X^\delta, L_X^\delta]$, with $L_X^\delta \uparrow +\infty$ as $\delta \downarrow 0$. Thus S^δ is a finite set of equally δ-spaced points denoted by $\{x_{-N}, \dots, x_N\}$, where $N = [L_X^\delta \delta^{-1}]$. We also introduce the nondimensional spacing $\delta' = \delta\tau_0^{1/2} = \delta\Delta^{-1}\sqrt{\Gamma}$.

The process X is stepwise constant over time intervals whose durations are independent and identically distributed with the exponential distribution with parameter $\Lambda = 2\tau^{-2}\delta^{-2}$. At the jump times the process randomly jumps to one of its nearest neighbors. If it is at position x, then the process jumps to the right neighbor $x + \delta$ with probability $\alpha_x = \frac{1}{2}(1 - \frac{\tau\delta x}{2})$ and it jumps to the left neighbor $x - \delta$ with probability $1 - \alpha_x$ (except when it is at the boundaries of its state space where it deterministically jumps to its unique nearest neighbor). The stochastic simulation method to generate trajectories of X is described in Appendix A.

The process X can be seen as a discretization of an Ornstein-Uhlenbeck (OU) process with correlation time $\tau > 0$. In [14] it is proved that the process X converges in distribution to $X^\star$ as $\delta \to 0$, where $X^\star$ is an OU process, which is the solution of the stochastic differential equation

$$\tau\dot{X}^\star = -X^\star + \sqrt{2}\dot{W}, \tag{6}$$

with $\dot{W}$ a white noise. The OU process $X^\star$ is a stationary zero-mean Gaussian process with correlation function $\mathbb{E}[X^\star(0)X^\star(t)] = (1/\tau)\exp(-|t|/\tau)$. From the dimensional analysis of Sec. II and the expression of the nondimensional spacing δ', we can actually approximate the distribution of X by the distribution of $X^\star$ when δ' is much smaller than 1. This means that X is indeed a discretization of the OU process $X^\star$ with correlation time τ. Additionally, when τ' is much smaller than 1, then $X^\star$ behaves like the white noise $\sqrt{2}\dot{W}$.

B. Description of the PDMP

We now define the PDMP modeling dry friction driven by the noise X. The PDMP is the process $Z = (X, Y, V)$. The coordinate X is the jump process modeling the driving force described above. The coordinate V is the continuous process defined by (2) or (3). The coordinate Y is the jump process determined by $Y = \Theta(X, V)$, with

$$\Theta(x, v) = \begin{cases} 1 & \text{if } v > 0 \text{ or if } v = 0,\ \sqrt{\Gamma}x > -\mathfrak{b}(0) + \Delta, \\ -1 & \text{if } v < 0 \text{ or if } v = 0,\ \sqrt{\Gamma}x < -\mathfrak{b}(0) - \Delta, \\ 0 & \text{if } v = 0,\ \sqrt{\Gamma}x \in [-\mathfrak{b}(0) - \Delta, -\mathfrak{b}(0) + \Delta]. \end{cases} \tag{7}$$

The marker Y indicates whether the process is in a dynamic phase ($|Y| = 1$) or in a static phase ($Y = 0$). The introduction of the marker Y makes it possible to adopt the formalism of PDMPs, with smooth flows for the continuous process V and jumps of the mode (X, Y) that occur at random times when X jumps and when the dynamics for V changes from the static to the dynamic phases. We give details on the definition of the PDMP Z in Appendix B. This formalism allows us to use the theory and simulation methods developed for PDMPs described in Refs. [15,16], and it will allow us to introduce representation formulas for quantities of interest using a strong Markov property.

It is proved in [14] that the random process (X, V) converges in distribution to the Markov process $(X^\star, V^\star)$, which is solution of (6)–(3). So we can consider the process (X, V) as a discretization of the process $(X^\star, V^\star)$.

C. Definition of long excursions

A long excursion is composed of two parts which we call half-long excursions (HLEs). We define the two integers k_- and k_+ by $\sqrt{\Gamma}x_{k_+} \leqslant -\mathfrak{b}(0) + \Delta < \sqrt{\Gamma}x_{k_+ + 1}$ and $\sqrt{\Gamma}x_{k_- - 1} < -\mathfrak{b}(0) - \Delta \leqslant \sqrt{\Gamma}x_{k_-}$. The two integers k_- and k_+ play important roles because a transition from a static phase to a dynamic phase occurs when Z jumps from $(x_{k_+}, 0, 0)$ to $(x_{k_+ + 1}, 1, 0)$ or from $(x_{k_-}, 0, 0)$ to $(x_{k_- - 1}, -1, 0)$. We can define the first HLE originating from $(x_{k_+ + 1}, 1, 0)$ as a portion of trajectory of the process Z starting from $(x_{k_+ + 1}, 1, 0)$ at time 0 and ending in $(x_{k_- - 1}, -1, 0)$ at time $t_{\frac{1}{2}} = \inf\{t \geqslant 0,\ V(t) = 0 \text{ and } X(t) = x_{k_- - 1}\}$. The second HLE starts from $(x_{k_- - 1}, -1, 0)$ at time $t_{\frac{1}{2}}$ and ends in $(x_{k_+ + 1}, 1, 0)$ at the time $t_1 = \inf\{t \geqslant t_{\frac{1}{2}},\ V(t) = 0 \text{ and } X(t) = x_{k_+ + 1}\}$. We use the notation $\pm$-HLE for a half-long excursion originating from $(x_{k_\pm \pm 1}, \pm 1, 0)$ (see Fig. 2). In general, a long excursion is defined as the concatenation of a $\pm$-HLE followed by a $\mp$-HLE. It is worth noting that it is possible that such an HLE evolves only in a dynamic phase. Long excursions are building blocks for the forthcoming representation formulas for quantities of interest such as the diffusivity.

IV. MOBILITY AND DIFFUSIVITY

In this section we propose original representation formulas for the displacement mobility and diffusivity in terms of a long excursion. These formulas will then be used to build efficient estimators of the diffusivity in the next section. We

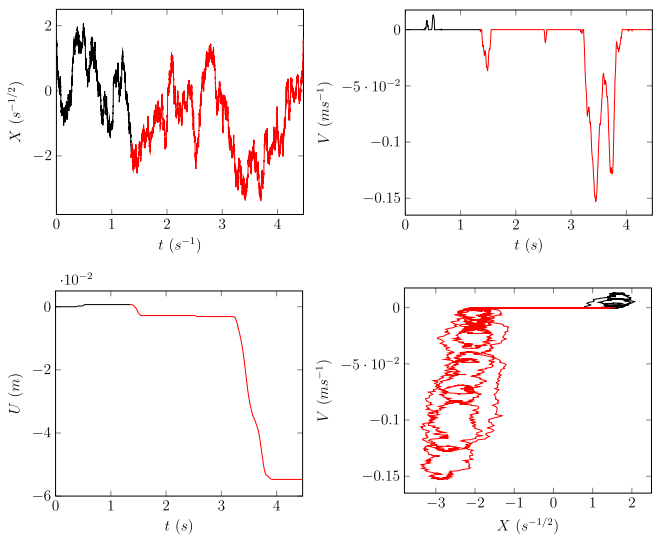

FIG. 2. Numerical simulation of a long excursion of (X, V) enclosed by the random time interval $[0, t_1]$. The first HLE in black is followed by the second HLE in red. Top left: Noise X vs time t. Top right: Velocity V vs time t. Bottom left: Displacement U vs time t. Bottom right: Velocity V vs noise X. Here $\mathfrak{b}(v) = -v/\tau_L + \bar{\gamma}$, $\tau = 0.5\,\mathrm{s}$, $\tau_L = 0.067\,\mathrm{s}$, $\Delta = 3.84\,\mathrm{m\,s^{-2}}$, $\Gamma = 5\,\mathrm{m^2\,s^{-3}}$, and $\bar{\gamma} = 0.342\,\mathrm{m\,s^{-2}}$. This sample is produced by Algorithm 1 with $\delta = 0.125\,\mathrm{s}^{-1/2}$.

consider the displacement $U(t)$. It satisfies the two following properties:

(1) $U(t)/t$ converges in probability as $t \to +\infty$ to

$$M_0 = \frac{\mathbb{E}_{s_+}[U(t_1)]}{\mathbb{E}_{s_+}[t_1]}, \tag{8}$$

where $\mathbb{E}_{s_+}$ stands for the expectation with respect to the distribution of the PDMP starting from $s_+ = (x_{k_+ +1}, 1, 0)$.

(2) $\sqrt{t}[U(t)/t - M_0]$ converges in distribution as $t \to +\infty$ to a Gaussian variable with mean zero and variance

$$D = \frac{\mathrm{Var}_{s_+}[U(t_1)]}{\mathbb{E}_{s_+}[t_1]}. \tag{9}$$

We will show in the following sections that the two representation formulas (8) and (9) make it possible to build unbiased and consistent Monte Carlo estimators. The remainder of this section is devoted to the proof of (8) and (9), which is based on standard limit theorems (law of large numbers and central limit theorem) and a strong Markov property.

Proof of (8) and (9). We introduce $s_- = (x_{k_- -1}, -1, 0)$, $t_0 = 0$, and for $j \geqslant 0$: $t_{j+1} = \inf\{t \geqslant t_{j+1/2}, [X(t), Y(t), V(t)] = s_+\}$, $t_{j+1/2} = \inf\{t \geqslant t_j, [X(t), Y(t), V(t)] = s_-\}$,

$$J_t = \inf\{j \geqslant 1,\ t_j \geqslant t\}, \quad j_t = \left\lfloor \frac{t}{\mathbb{E}_{s_+}[t_1]} \right\rfloor,$$

where $\lfloor \cdot \rfloor$ stands for the integer part. The random variables

$$\mathcal{X}_j = \int_{t_j}^{t_{j+1}} V(s)ds$$

are independent and identically distributed as $\mathcal{X}_0 = U(t_1)$ under $\mathbb{E}_{s_+}$ by the strong Markov property. If $\mathfrak{b}$ is an odd function, then $\mathbb{E}_{s_+}[\mathcal{X}_0] = 0$ (this can be shown by a symmetry argument, because $(X_t, V_t)_{t\geqslant 0}$ has then the same distribution as $(-X_t, -V_t)_{t\geqslant 0}$), but in general it is not zero.

We have

$$\frac{1}{t}U(t) = \frac{j_t}{t}\left[\frac{1}{j_t}\sum_{j=0}^{j_t-1}\mathcal{X}_j + R_t\right],$$

with

$$R_t = \frac{1}{j_t}\int_{t_{j_t}}^{t} V(s)ds.$$

We show in Appendix C that $\sqrt{t}R_t$, and hence R_t, converges in probability to zero as $t \to +\infty$. Moreover, $j_t \to \infty$ as $t \to +\infty$, so we obtain from the law of large numbers that ${j_t}^{-1}\sum_{j=0}^{j_t-1}\mathcal{X}_j$ converges in probability to $\mathbb{E}_{s_+}[\mathcal{X}_0]$. We also observe that $j_t/t \to 1/\mathbb{E}_{s_+}[t_1]$. Therefore we obtain

$$\frac{1}{t}U(t) \xrightarrow{\text{proba.}} M_0 = \frac{\mathbb{E}_{s_+}[\mathcal{X}_0]}{\mathbb{E}_{s_+}[t_1]}, \tag{10}$$

which gives (8). In order to show (9), we write

$$\sqrt{t}\left(\frac{U(t)}{t} - M_0\right) = \frac{\sqrt{j_t}}{\sqrt{t}}\left[\frac{1}{\sqrt{j_t}}\sum_{j=0}^{j_t-1}\tilde{\mathcal{X}}_j + \tilde{R}_t\right] + \tilde{r}_t,$$

with $\tilde{\mathcal{X}}_j = \mathcal{X}_j - \mathbb{E}_{s_+}[\mathcal{X}_0]$,

$$\tilde{R}_t = \sqrt{t}R_t = \frac{1}{\sqrt{j_t}}\int_{t_{j_t}}^{t} V(s)ds,$$

$$\tilde{r}_t = \frac{j_t}{\sqrt{t}}\mathbb{E}_{s_+}[\mathcal{X}_0] - \sqrt{t}M_0.$$

We show in Appendix C that $\tilde{R}_t$ converges in probability to zero as $t \to +\infty$. The quantity $\tilde{r}_t = \mathbb{E}_{s_+}[\mathcal{X}_0](\lfloor t/\mathbb{E}_{s_+}[t_1]\rfloor - t/\mathbb{E}_{s_+}[t_1])/\sqrt{t}$ is such that $|\tilde{r}_t| \leqslant |\mathbb{E}_{s_+}[\mathcal{X}_0]|/\sqrt{t}$ so it also converges to zero as $t \to +\infty$. Since $\tilde{\mathcal{X}}_j$ are independent and identically distributed with mean zero, we obtain from the central limit theorem that ${j_t}^{-1/2}\sum_{j=0}^{j_t-1}\tilde{\mathcal{X}}_j$ converges in distribution to a zero-mean Gaussian variable with variance $\mathrm{Var}_{s_+}(\mathcal{X}_0)$. We also observe that $\sqrt{j_t}/\sqrt{t} \to 1/\sqrt{\mathbb{E}_{s_+}[t_1]}$. By Slutsky's theorem we obtain

$$\sqrt{t}\left(\frac{U(t)}{t} - M_0\right) \xrightarrow{dist.} \mathcal{N}(0, D), \quad D = \frac{\mathrm{Var}_{s_+}(\mathcal{X}_0)}{\mathbb{E}_{s_+}[t_1]}, \tag{11}$$

which completes the proof of the desired result. ■

V. MONTE CARLO ESTIMATION OF THE DIFFUSIVITY

A. Monte Carlo estimator based on long excursions

Consider a long excursion as defined in Sec. III C. It is composed of two HLEs. We can now introduce an original Monte Carlo method for the estimation of D. Let $(U_{\mathrm{le}}^{(k)}, t_{\mathrm{le}}^{(k)})$, $k = 1, \ldots, N$, be N independent and identically distributed (i.i.d.) pairs of displacement $U(t_1)$ and duration t_1, both resulting from a long excursion. We introduce a Monte Carlo estimator based on long excursions as follows:

$$\hat{D}_N = \frac{\sum_{k=1}^N \left(U_{\mathrm{le}}^{(k)}\right)^2 - \frac{1}{N}\left(\sum_{k=1}^N U_{\mathrm{le}}^{(k)}\right)^2}{\sum_{k=1}^N t_{\mathrm{le}}^{(k)}}. \tag{12}$$

Algorithm 1. PDMP simulation for the first HLE from $(x_{k_++1}, 1, 0)$ to $(x_{k_--1}, -1, 0)$.

Result: Simulation of $\{(X, Y, V)_{T_j}$ where $j \geqslant 0$ and $T_j \leqslant t_{\frac{1}{2}}\}$.
$T = 0$, $X = x_{k_++1}$, $Y = 1$, $V = 0$, $U = 0$, $A =$ TRUE;
while A **do**
  $\delta T =$ interjump(X, Y, V);
  $U = U +$displacement$(X, Y, V, T, T + \delta T)$;
  $(X, Y, V) =$ jump$(X, Y;$ flow$(X, Y, V; \delta T))$;
  $T = T + \delta T$;
  $A = (X \neq x_{k_--1})$ or $(Y \neq -1)$ or $(V \neq 0)$;
end

The sample $\{(U_{\rm le}^{(k)}, t_{\rm le}^{(k)})\}_{k=1}^N$ is produced by using Algorithm 1. The estimator $\hat{D}_N$ is consistent by the law of large numbers. Beyond the estimator $\hat{D}_N$, it is possible to build from the sample $\{(U_{\rm le}^{(k)}, t_{\rm le}^{(k)})\}_{k=1}^N$ a confidence interval with prescribed asymptotic confidence level α (see Appendix D).

To simulate the other HLE, we can swap x_{k_++1} with x_{k_--1}, $(Y = 1)$ with $(Y = -1)$, and vice versa in Algorithm 1. The functions interjump (X, Y, V), displacement (X, Y, V), flow $(X, Y, V, \delta T)$ (which is used in displacement (X, Y, V)) and jump$(X, Y; V)$ are described in Appendix E.

B. Brute force Monte Carlo estimator

For comparison, we also consider the brute force Monte Carlo estimator for D, that is

$$\hat{D}_{N'}^t = \frac{1}{t}\left[\frac{1}{N'}\sum_{k=1}^{N'} U^{(k)}(t)^2 - \left(\frac{1}{N'}\sum_{k=1}^{N'} U^{(k)}(t)\right)^2\right], \qquad (13)$$

where the sample $\{U^{(k)}(t)\}_{k=1}^{N'}$ is composed of N' i.i.d. realizations of the displacement at time t and is produced by using Algorithm 2. Note that $\hat{D}_{N'}^t$ is actually a consistent estimator of D^t. This means that t should be chosen large enough so that the bias (the difference between D^t and D) is negligible. We discuss this point in detail in Sec. V C.

C. Asymptotic efficiencies of the estimators

In this section we show that the mean square error of the estimator $\hat{D}_N$ based on long excursions is much smaller than that of the brute force Monte Carlo estimator $\hat{D}_N^t$, even when tuning the parameter t optimally.

Algorithm 2. PDMP simulation on $[0, t]$.

Result: Simulation of $\{(X, Y, V)_{T_j}$ where $j \geqslant 0$ and $T_j \leqslant t\}$.
$T = 0$, $X = x_{k_++1}$, $Y = 0$, $V = 0$, $U = 0$;
while $(T < t)$ **do**
  $\delta T =$ interjump(X, Y, V);
  $U = U +$ interjump(X, Y, V);
  $(X, Y, V) =$jump$(X, Y;$flow$(X, Y, V; \delta T))$;
  $T = T + \delta T$;
  if $(T \geqslant t)$ **then** $U = U +$ displacement$(X, Y, V, T - \delta T, t)$;
end

From the delta method (described in Appendix D), the mean square error of the estimator $\hat{D}_N$ satisfies

$$\mathbb{E}_{s_+}\left[(\hat{D}_N - D)^2\right] \sim \frac{\sigma^2}{N}, \qquad (14)$$

as $N \to +\infty$, where the variance $\sigma^2 = \nabla\Psi(\boldsymbol{S})^T \mathbf{C} \nabla\Psi(\boldsymbol{S})$ involves $\boldsymbol{S} = \mathbb{E}_{s_+}[\boldsymbol{X}]$, $\mathbf{C} = (C_{jl})_{j,l=1}^3$, $C_{jl} = \mathbb{E}_{s_+}[X_j X_l] - \mathbb{E}_{s_+}[X_j]\mathbb{E}_{s_+}[X_l]$, $\Psi(\boldsymbol{x}) = \frac{x_2 - x_1^2}{x_3}$ with $\boldsymbol{X} = (X_j)_{j=1}^3$, $X_1 = U_{\rm le} = U(t_1)$, $X_2 = {U_{\rm le}}^2 = U(t_1)^2$, $X_3 = t_{\rm le} = t_1$.

The mean square error of the estimator $\hat{D}_{N'}^t$ satisfies

$$\mathbb{E}_{s_+}\left[\left(\hat{D}_{N'}^t - D\right)^2\right] \sim \frac{(\sigma^t)^2}{N'} + (D^t - D)^2, \qquad (15)$$

as $N' \to \infty$, where $(\sigma^t)^2 = \nabla\Phi(\boldsymbol{R})^T \boldsymbol{\Gamma} \nabla\Phi(\boldsymbol{R})$ involves $\boldsymbol{R} = \mathbb{E}_{s_+}[\boldsymbol{Y}]$, $\boldsymbol{\Gamma} = (\Gamma_{jl})_{j,l=1}^2$, $\Gamma_{jl} = \mathbb{E}_{s_+}[Y_j Y_l] - \mathbb{E}_{s_+}[Y_j]\mathbb{E}_{s_+}[Y_l]$, $\Phi(\boldsymbol{y}) = y_2 - y_1^2$ with $\boldsymbol{Y} = (Y_j)_{j=1}^2$, $Y_1 = U(t)/\sqrt{t}$, $Y_2 = U(t)^2/t$. Note that the mean square error is the sum of a variance term and a squared bias term. The latter turns out to have a dramatic effect.

Denoting $\overline{t_1} = \mathbb{E}_{s_+}(t_1)$, it takes $\sum_{k=1}^N t_{\rm le}^{(k)} \approx N\overline{t_1}$ computational time units to produce the sample $\{(U_{\rm le}^{(k)}, t_{\rm le}^{(k)})\}_{k=1}^N$ and $N't$ computational time units to produce the sample $\{(U^{(k)}(t)\}_{k=1}^{N'}$. Therefore, when $t = \alpha\overline{t_1}$, we consider the relation $N'\alpha = N$ in order to compare $\hat{D}_N$ and $\hat{D}_{N'}^t$(which becomes $\hat{D}_{N/\alpha}^{\alpha\overline{t_1}}$) with identical computational cost. With $t = \alpha\overline{t_1}$, the mean square error of the estimator $\hat{D}_{N/\alpha}^{\alpha\overline{t_1}}$ satisfies

$$\mathbb{E}_{s_+}\left[\left(\hat{D}_{N/\alpha}^{\alpha\overline{t_1}} - D\right)^2\right] \sim \frac{\alpha(\sigma^{\alpha\overline{t_1}})^2}{N} + (D^{\alpha\overline{t_1}} - D)^2,$$

as $N \to \infty$. We want to compare the mean square errors of the estimators $\hat{D}_N$ and $\hat{D}_N^t$. First, we need to tune the parameter t to get the minimal error.

We first consider the case when $M_0 = 0$. When α becomes large, $(\sigma^{\alpha\overline{t_1}})^2$ converges to $2D^2$. When α becomes large, we have $D^{\alpha\overline{t_1}} = D + O(\alpha^{-1})$. Indeed,

$$D^t = \frac{2}{t}\int_0^t \int_0^{t-s} \mathrm{Cov}_{s_+}(V(s), V(s+s'))ds'ds,$$

$\mathrm{Cov}_{s_+}(V(s), V(s+s'))$ converges exponentially as $s \to +\infty$ to an integrable function $\phi(s')$, which is the stationary covariance function of V (see Fig. 5) and $D = \lim_{t\to+\infty} D^t = 2\int_0^\infty \phi(s')ds'$ so that

$$\begin{aligned}
&\frac{t}{2}(D^t - D)\\
&\quad = \int_0^t \int_0^\infty [\mathrm{Cov}_{s_+}(V(s), V(s+s'))\mathbf{1}_{s'<t-s} - \phi(s')]ds'ds\\
&\quad \overset{t\to+\infty}{\longrightarrow} \int_0^\infty \int_0^\infty [\mathrm{Cov}_{s_+}(V(s), V(s+s')) - \phi(s')]ds'ds\\
&\qquad - \int_0^\infty s'\phi(s')ds'.
\end{aligned}$$

For $t = \alpha\overline{t_1}$ we define $\alpha_N^\star$ the minimizer of the function $\alpha \mapsto N^{-1}\alpha(\sigma^{\alpha\overline{t_1}})^2 + (D^{\alpha\overline{t_1}} - D)^2$. By the two previous observations about the asymptotic behaviors of $\sigma^{\alpha\overline{t_1}}$ and $D^{\alpha\overline{t_1}} - D$, we find that $\alpha_N^\star$ is of the order of $\alpha_N^\star \sim N^{1/3}$ so that the

minimal mean square error of $\hat{D}_{N/\alpha}^{\alpha t_1}$ obtained with $\alpha_N^\star$ is of order $N^{-2/3}$. That means that, even when tuning the brute force Monte Carlo with the optimal t, its mean square error is larger than the mean square error of $\hat{D}_N$, which is of order N^{-1} without any tuning. This shows that the estimator $\hat{D}_N$ is clearly preferable in the regime when N is large.

When $M_0 \neq 0$, the situation is even worse for the brute force Monte Carlo estimator, because $(\sigma^t)^2$ becomes equivalent to $M_0^2 Dt$ for large t, so that the optimal $\alpha_N^\star \sim N^{1/4}$ and the minimal mean square error of $\hat{D}_{N/\alpha}^{\alpha t_1}$ obtained with $\alpha_N^\star$ is of order $N^{-1/2}$.

This is the main output of this paper from the methodological point of view: the estimation of the diffusivity (or mobility or any other asymptotic quantity) should be carried out with the Monte Carlo method based on long excursions, rather than the Monte Carlo method based on long fixed-time excursions that is traditionally used in the literature.

VI. LIMITING DIFFERENTIAL INCLUSION

In this section the notion of long excursion and the corresponding sampling approach are extended to the limiting differential inclusion case.

A. Long excursion of the differential inclusion

From [14], the PDMP (X, V) converges in distribution as $\delta \to 0$ towards $(X^\star, V^\star)$ the solution of the differential inclusion:

$$\dot{V}^\star + \partial\varphi(V^\star) \ni \mathfrak{b}(V^\star) + \sqrt{\Gamma} X^\star, \tag{16}$$

where $\tau \dot{X}^\star = -X^\star + \sqrt{2}\dot{W}$ and $\varphi(v) = \Delta|v|$. The process $X^\star$ is an OU process, and its invariant density is a Gaussian distribution with mean zero and variance τ^{-1}.

It is natural to extend the concepts of long excursion to the limiting differential inclusion case. The definitions of half-long and long excursions for $(X^\star, V^\star)$ are similar to those of (X, V) defined in Sec. III C. The first HLE for $(X^\star, V^\star)$ starts at time 0 from $(x_\Delta, 0)$ and ends at time $t_{1/2}^\star = \inf\{t \geqslant 0, X^\star(t) = x_{-\Delta} \text{ and } V^\star(t) = 0\}$. Then the second HLE for $(X^\star, V^\star)$ starts at time $t_{1/2}^\star$ from $(x_{-\Delta}, 0)$ and ends at time $t_1^\star = \inf\{t \geqslant t_{1/2}^\star, X^\star(t) = x_\Delta \text{ and } V^\star(t) = 0\}$. Here, we have introduced the points $x_\Delta = (-\mathfrak{b}(0) + \Delta)/\sqrt{\Gamma}$ and $x_{-\Delta} = (-\mathfrak{b}(0) - \Delta)/\sqrt{\Gamma}$.

The diffusivity $D^\star$ is defined as in (1) but with $\dot{U}^\star = V^\star$. It has the following representation formula in terms of the long excursion:

$$D^\star = \frac{\mathrm{Var}_{(x_\Delta,0)}[U^\star(t_1^\star)]}{\mathbb{E}_{(x_\Delta,0)}[t_1^\star]}. \tag{17}$$

B. Monte Carlo estimator

In this section we define a Monte Carlo (MC) estimator $\hat{D}_N^\star$ of the diffusivity $D^\star$. This estimator is based on the representation formula (17) in terms of the long excursions of the differential inclusion (in a similar manner to what was done for $\hat{D}_N$).

Algorithm 3. Differential inclusion simulation for the first HLE from $(x_\Delta, 0)$ to $(x_{-\Delta}, 0)$.

Result: $(X^\star, V^\star)$ on the interval $[0, t_{1/2}^\star]$.
$X^\star = x_\Delta,\ V^\star = 0,\ f^\star = 0,\ U^\star = 0,\ A = \text{TRUE}$;
while A **do**
  $(\hat{\Xi}, \hat{X})^T \sim \mathcal{N}(X^\star m(h), \Sigma(h))$;
  $(\hat{f}, \hat{V}) = (f^\star, V^\star)$;
  $f^\star = \hat{V} + h(\mathfrak{b}(\hat{V}) + \sqrt{\Gamma}\hat{\Xi})$;
  $V^\star = \hat{V} - h\max(-\Delta, \min(\Delta, \hat{f}h^{-1}))$;
  $X^\star = \hat{X}$; $U^\star = U^\star + h\hat{V}$;
  $A = (|\hat{f}| > \Delta)$ or $(\hat{V} \neq 0)$ or $f^\star \leqslant -\Delta$;
end

Let $\{U_{\mathrm{le}}^{\star,(k)}, t_{\mathrm{le}}^{\star,(k)}\}_{k=1}^N$ be N i.i.d. pairs of displacement and duration resulting from a long excursion. This sample is produced by Algorithm 3.

Here the notation $(\hat{\Xi}, \hat{X})^T \sim \mathcal{N}(xm(h), \Sigma(h))$ means that $(\hat{\Xi}, \hat{X})^T$ is a realization of a two-dimensional Gaussian variable with expectation $xm(h)$ with

$$m(h) = \left(\frac{\tau}{h}\left(1 - e^{-h/\tau}\right), e^{-h/\tau}\right)^T$$

and with covariance matrix

$$\Sigma(h) = \begin{pmatrix} \frac{\tau}{h^2}\left(2\frac{h}{\tau} - 3 + 4e^{-h/\tau} - e^{-2h/\tau}\right) & \frac{1}{h}\left(1 - e^{-h/\tau}\right)^2 \\ \frac{1}{h}\left(1 - e^{-h/\tau}\right)^2 & \frac{1}{\tau}\left(1 - e^{-2h/\tau}\right) \end{pmatrix}.$$

In fact, the Gaussian distribution $\mathcal{N}(xm(h), \Sigma(h))$, which is used at every time step, is the law of the two-dimensional random vector

$$\left(\frac{1}{h}\int_0^h X_s^{\star,x} ds, X_h^{\star,x}\right), \tag{18}$$

where we use the notation $X_h^{\star,x}$ for the state of the OU noise variable at time h provided that it started from x at time 0.

The MC estimator $\hat{D}_N^\star$ and a confidence interval for $D^\star$ are built from the sample $\{U_{\mathrm{le}}^{\star,(k)}, t_{\mathrm{le}}^{\star,(k)}\}_{k=1}^N$ by using Eq. (12) and Appendix D.

VII. NUMERICAL RESULTS

This section is devoted to numerical results produced by the algorithms presented in the previous section. We study the sensitivity of the diffusivity D with respect to the strength of the noise Γ and the correlation time τ.

Simulation parameters. In the results shown below, the differential inclusion (16) is integrated with a time step of $h = 10^{-4}$ s. Each Monte Carlo result is produced with $N = 10^5$.

A. Comparisons between PDMP and differential inclusion simulations

In Fig. 3 we present a sample of long excursion related to the PDMP (X, V) defined in Sec. III and the solution of the differential inclusion $(X^\star, V^\star)$ defined by Eq. (16) when $\mathfrak{b}(v) = -v/\tau_L + \bar{\gamma}$. Here $\delta = 0.125\,\mathrm{s}^{-1/2}$ and $\delta' \simeq 0.073$, which is smaller than 1, so we can expect that the distribution of the PDMP solution is close to that of the limiting differential inclusion. Indeed, in Fig. 3 the two trajectories have

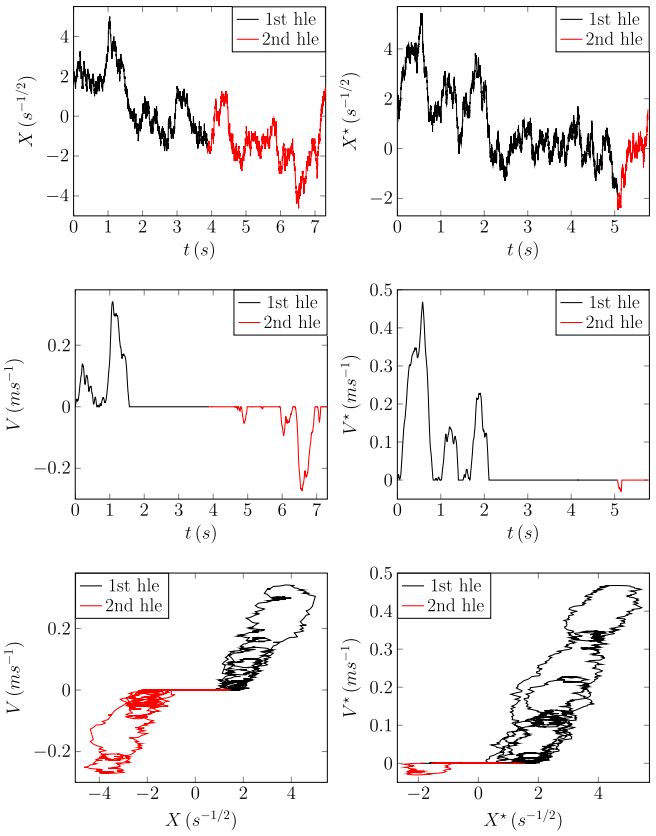

FIG. 3. Numerical stochastic dynamics of a long excursion when $\mathfrak{b}(v) = -v/\tau_L + \bar{\gamma}$. Left column: Single long excursion simulation of the PDMP (X, V) with $\delta = 0.125\,\mathrm{s}^{-1/2}$. Right column: Single long excursion simulation of the solution of the differential inclusion. Here $\tau = 0.5\,\mathrm{s}$, $\tau_L = 0.067\,\mathrm{s}$, $\Delta = 3.84\,\mathrm{ms}^{-2}$ and $\Gamma = 5\,\mathrm{m}^2\,\mathrm{s}^{-3}$, and $\bar{\gamma} = 0.342\,\mathrm{ms}^{-2}$.

similar behaviors to the naked eye. In Fig. 4 we superpose the computed diffusivity and the mean duration of long excursions of both (X, V) and $(X^\star, V^\star)$ when $\Gamma \in [1, 10]\,\mathrm{m}^2\,\mathrm{s}^{-3}$ and $\tau = 0.125, 0.25, 0.5, 1\,\mathrm{s}$. Then in Fig. 5 we also compute the empirical covariance for each process. In agreement with the theory, the statistics of (X, V) are close to those of $(X^\star, V^\star)$ when δ is small enough (i.e., when δ' is smaller than 1).

Comments. The PDMP makes the mathematical framework for the diffusivity very neat. However, one drawback in simulating the PDMP appears when we consider τ small. Indeed, the jump frequency of the PDMP becomes very high, and therefore its dynamics evolves with extremely small time steps. In this context the CPU time becomes significantly important. This is the reason why we extend the notion of long excursion to the limit process in its differential inclusion form.

B. Comparisons between white-noise and colored-noise regimes

Here we assume that $\mathfrak{b}(v) = -v/\tau_L + \bar{\gamma}$, and we carry out simulations with the limiting differential inclusion. As illustrated in Fig. 6 (left), the numerically obtained stationary probability for the colored noise with $\tau = 10^{-5}\,\mathrm{s}$ agrees with the explicit formula (valid for a white noise) of the theoretical stationary probability [19] of the velocity $P(v) =$

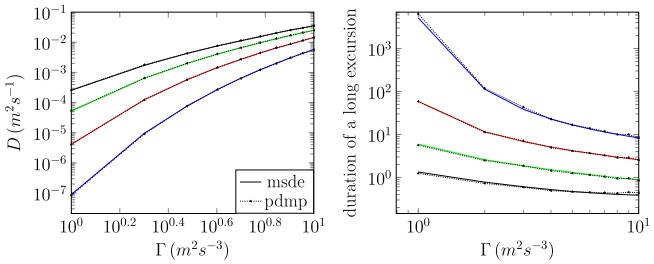

FIG. 4. Left: Monte Carlo estimation of the diffusivity D as a function of $\Gamma \in [1, 10]\ \mathrm{m}^2\,\mathrm{s}^{-3}$ in loglog scale when $\mathfrak{b}(v) = -v/\tau_L + \bar{\gamma}$. The dots correspond to numerical simulations of the MC estimator $\hat{D}_N$ based on the PDMP long excursions when $\delta = 0.125\,\mathrm{s}^{-1/2}$, and the solid lines correspond to the MC estimator $\hat{D}_N^\star$ based on the long excursions of the limiting differential inclusion as $\delta \to 0$. The four curves from top to bottom correspond to $\tau = 0.125, 0.25, 0.5, 1\,\mathrm{s}$ and we have $\tau_L = 0.067\,\mathrm{s}$, $\Delta = 3.84\,\mathrm{ms}^{-2}$, and $\bar{\gamma} = 0.342\,\mathrm{ms}^{-2}$. Right: Monte Carlo estimation of the mean duration of a long excursion as a function of Γ in loglog scale. The four curves from bottom to top correspond to $\tau = 0.125, 0.25, 0.5, 1\,\mathrm{s}$. The parameters remain unchanged compared to the left figure.

$P_0 e^{-v^2/(\Gamma\tau_L) - 2|v|\Delta/\Gamma + 2v\bar{\gamma}/\Gamma}$, and $P_0 > 0$ is a normalizing constant. The white-noise regime is indeed expected, since $\tau' \simeq 9.2 \times 10^{-4}$ is much smaller than 1. In addition, some realizations of the dynamics of $U(t)$ are shown for $\tau = 10^{-5}\,\mathrm{s}$ in Fig. 6 (right). We observe an average positive drift due to the presence of $\bar{\gamma}$. This is a good qualitative agreement with Fig. 2 of [13].

Here we consider the pure dry friction $\mathfrak{b}(v) = 0$, and we want to compare our numerical results with the theoretical predictions of [5], valid in the white-noise regime. We here consider the system in nondimensional variables. The numerically obtained histogram, first moment, and correlation function for the velocity $\check{V}^{\star,\prime}(t')$ are shown for several values of the noise correlation time τ' ($\tau' = 0.5 \times 10^{-i}$, $1 \leqslant i \leqslant 4$) in Fig. 7, Table I, and Fig. 8, respectively. As $\tau' \to 0$, all our simulation results capture the predictions of [5] [see formulas

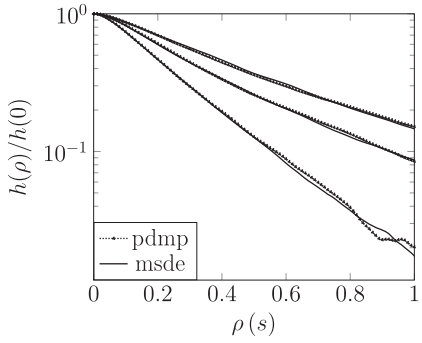

FIG. 5. $h(\rho)/h(0)$ on a semilog scale where $h(\rho) = \mathrm{cov}(V(t), V(t+\rho))$ when $\mathfrak{b}(v) = -v/\tau_L + \bar{\gamma}$. The solid lines stand for the empirical covariances obtained by PDMP simulations. The dotted lines stand for the empirical covariances obtained by MSDE simulations. The three curves from bottom to top correspond to $\tau = 0.25,\ 0.5,\ 1\,\mathrm{s}$ (i.e., $\tau' = 0.74,\ 1.47,\ 2.95$). Here $\tau_L = 0.067\,\mathrm{s}$, $\Delta = 3.84\,\mathrm{ms}^{-2}$, $\Gamma = 5\,\mathrm{m}^2\,\mathrm{s}^{-3}$, $\bar{\gamma} = 0.342\,\mathrm{ms}^{-2}$, and $\delta = 0.125\,\mathrm{s}^{-1/2}$ (for the PDMP).

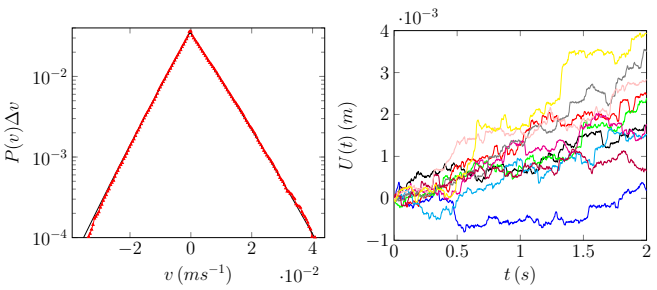

FIG. 6. Left: Comparison between the theoretical stationary probability $P(v)\Delta v$ in solid line and the numerical histogram of the velocity with bin width $\Delta v = 4.8 \times 10^{-4}\,\mathrm{ms}^{-1}$ in red triangles for the colored-noise-driven system when $\mathfrak{b}(v) = -v/\tau_L + \bar{\gamma}$. Right: Displacement $U(t)$ vs t for a colored-noise-driven system. Ten simulations are plotted on $t \in [0, 2]$ s. Here $\tau = 10^{-5}$ s, $\Gamma = 0.16\,\mathrm{m}^2\,\mathrm{s}^{-3}$, $\Delta = 3.84\,\mathrm{ms}^{-2}$, $\tau_L = 0.067$ s, and $\bar{\gamma} = 0.342\,\mathrm{ms}^{-2}$.

(2.10), (2.11), and (2.13) therein]. We can see, however, a significant departure in Fig. 7 for $\tau' = 0.5 \times 10^{-1}$, which means that the white-noise approximation is no longer valid for such a value of the correlation time to give predictions of the statistics of the velocity.

As shown in the left side of Fig. 9, produced with $\mathfrak{b}(v) = 0$, the diffusivity varies as Γ^3 when $\tau = 10^{-j}$ s, $j = 4, 5$, i.e., $\tau' \simeq 2.9 \times 10^{-j}$, $j = 4, 5$ (close to white noise). Otherwise when τ gets larger ($\tau = 10^{-j}$ s, $j = 2, 3$), the relationship in log-log scale between D and Γ is not linear and thus there is no scaling law of the form $D \sim \Gamma^\alpha$ with a constant α. This means that the white-noise approximation is not valid anymore for $\tau' \simeq 2.9 \times 10^{-j}$, $j = 2, 3$ to study the diffusivity. The white-noise approximation should be used with caution, and even a

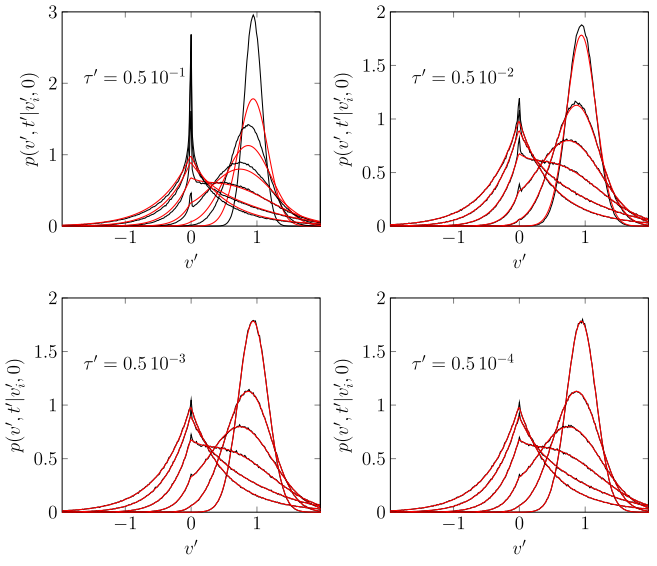

FIG. 7. Red curves: Probability density function $v' \mapsto p(v', t'|v_i', 0)$ of the velocity at different times t' for the white-noise-driven pure dry friction case with initial condition $v_i' = 1$ at time 0 in nondimensional variables (see Formula (2.10) in [5]). Black curves: Empirical histogram of the velocity for the colored-noise-driven pure dry friction with the initial condition is $v_i' = 1$ and $x_i' \sim \mathcal{N}(0, \tau'^{-1})$. The four plots are for four different values of the correlation time τ'.

TABLE I. First moment of $V^{\star,\prime}(t')$ vs t' for the pure dry friction case with initial condition $v_i' = 1$. The MC line results from our simulations with $\tau' = 0.5 \times 10^{-5}$. The EF line is the explicit formula (2.11) in [5].

t'	0.05	0.125	0.25	0.5	1	2.5
MC	0.950	0.876	0.757	0.569	0.337	0.091
EF	0.950	0.875	0.757	0.568	0.336	0.090

small correlation time of the driving force can have a strong impact. As shown in the right side of Fig. 9 produced with $\mathfrak{b}(v) = -v/\tau_L + \bar{\gamma}$, the same comment applies to all the cases for the relationship in log-log scale between D and Γ.

While we recover several theoretical results from Hayakawa [19], de Gennes [3], and Touchette *et al.* [4,5], we cannot say the same for the experimental results from [13]. In their experimental study we have $\mathfrak{b}(v) = -\tau_L^{-1} v + \bar{\gamma}$, where $\tau_L \simeq 0.067$ s is the momentum relaxation time, and $\bar{\gamma} \simeq 9.8 \sin(\pi/90) \simeq 0.342\,\mathrm{ms}^{-2}$ is a constant related to gravity and the inclination of the surface on which the system is installed. The noise in the experiment is assumed to be a white noise, and the friction coefficient Δ is estimated to be $3.84\,\mathrm{ms}^{-2}$. The experimentally obtained diffusivity scales as $\sim\Gamma^{1.61}$, which is not too far from their simulations, predicting a scaling $\sim\Gamma^{1.74}$ where the noise strength Γ varies between 5×10^{-3} and $5 \times 10^{-1}\,\mathrm{m}^2\,\mathrm{s}^{-3}$. When comparing with our results in Fig. 9 (right) we can observe a discrepancy. We believe that there are two possible (and related) explanations for such a discrepancy. First, the experimental and numerical forces are assumed to be white noises in [13], and we have exhibited above that the correlation time should be very small to ensure the validity of the white-noise approximation for the study of the diffusivity. We do not know the correlation time in the experiments, and the correlation time in the numerical simulations in [13] was apparently equal to the integration time step 10^{-3} s, which means that the white-noise approximation does not seem to be valid. Second, we have observed a high sensitivity of the numerical diffusivity to the integration time step itself. In our simulations we observed that the computa-

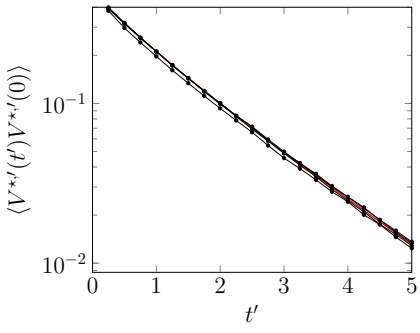

FIG. 8. Correlation function $\langle V^{\star,\prime}(t')V^{\star,\prime}(0)\rangle$ vs t' in semilog scale for the pure dry friction case under stationarity. The red solid line is the explicit formula (2.13) in [5] (valid when $\tau' \downarrow 0$). There are four curves in black dots from our simulations. The curves associated with the colored-noise case, where $\tau' = 0.5 \times 10^{-4}$, $\tau' = 0.5 \times 10^{-3}$, $\tau' = 0.5 \times 10^{-2}$, are almost indistinguishable. The remaining curve below the red curve is for $\tau' = 0.5 \times 10^{-1}$, and it is also very close to the first three ones.

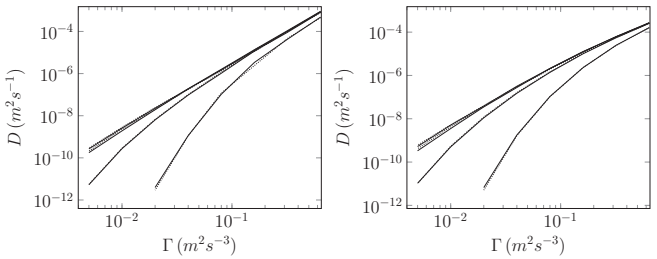

FIG. 9. Left: Case $\mathfrak{b}(v) = 0$. Right: Case $\mathfrak{b}(v) = -v/\tau_L + \bar{\gamma}$ with $\tau_L = 0.067\,\mathrm{s}$ and $\bar{\gamma} = 0.342\,\mathrm{ms}^{-2}$. The dots correspond to the numerical simulation of $\hat{D}_N^{t,\star}$ (the MC estimator based on the brute force simulation of the limiting differential inclusion with $t = 10\,\mathrm{s}$). The solid lines correspond to the numerical simulation of $\hat{D}_N^{\star}$ (the MC estimator based on the long excursion of the limiting differential inclusion). In both cases, the four curves from top to bottom correspond to $\tau = 10^{-i}\,\mathrm{s}$ for $i = 5, \ldots, 2$. Here $\Delta = 3.84\,\mathrm{ms}^{-2}$.

tion of the diffusivity in Fig. 9 appears to be more sensitive to the time step than the computation of the empirical histogram of the velocity in Fig. 7. Both Figs. 7 and 9 show results produced with $h = 10^{-4}\,\mathrm{s}$. We have observed that the results do not change when we take a smaller h. We have observed, however, that the results change when h reaches values of the order of $10^{-3}\,\mathrm{s}$. More exactly, the results of Fig. 7 do not vary much, but those of Fig. 9 vary significantly. It turns out that the acquisition time of the video recording in the experiments and the time step in the numerical simulations in [13] are both of this order of magnitude so it may explain the discrepancy. This observation strengthens the need of accurate simulation methods and makes the use of efficient Monte Carlo methods even more important in the context of expensive numerical simulations.

VIII. CONCLUSIONS

In this paper we have introduced a piecewise deterministic Markov process approach to model the random motion of an object subject to dry friction in presence of colored noise. The latter is represented by a pure jump process that is itself a δ spatial discretization of an Ornstein-Uhlenbeck noise with correlation time τ. In this model we have identified an independent and identically distributed sequence of repeating patterns or excursions. This excursion is the fundamental brick of the dynamics, because it encodes all the behavior of the system. We have shown that the variance of the object displacement has linear growth in time. We have obtained a representation formula for the diffusivity (the linear growth rate) as an expectation of a functional of an excursion. As a by-product, we have derived a Monte Carlo estimator for the diffusivity with much better properties that standard Monte Carlo estimators. The method we have developed can be used to calculate quantities similar to diffusivity (e.g., mobility etc) with high accuracy and confidence.

As the PDMP cannot be used for numerical purposes when τ and δ are small due to high frequency of jumps, we have extended the notion of excursion to the limit process as $\delta \downarrow 0$. When $\tau \downarrow 0$, all our numerical simulations for the stationary probability density function, the transition probability density function, the first moment, the correlation, and the diffusivity are captured by the theoretical predictions of Hayakawa [19], de Gennes [3], and Touchette *et al.* [4,5]. We have further investigated these quantities as functions of the correlation time τ of the noise. We have shown that the white-noise approximation gives correct predictions for the distribution of the velocity for small or moderately small values of the correlation time, but the white-noise approximation requires very small values of the correlation time to give correct predictions for the diffusivity.

ACKNOWLEDGMENTS

L.M. is thankful for support through NSFC Grant No. 12271364. The authors would like to thank Carl Xu for useful discussions.

APPENDIX A: THE DRIVING JUMP PROCESS

The random dynamics of X starting from a state $X(0) = \xi_0$ is as follows:

(1) Generate a random time τ_1 with an exponential distribution with parameter Λ. Set $X(t) = \xi_0$ for $t \in [0, \tau_1)$.

(2) If $|\xi_0| < x_N$, then with probability α_{ξ_0}, set $\xi_1 = \xi_0 + \delta$ and with probability $1 - \alpha_{\xi_0}$, set $\xi_1 = \xi_0 - \delta$.

If $\xi_0 = x_N$, then set $\xi_1 = x_{N-1}$.

If $\xi_0 = x_{-N}$, then set $\xi_1 = x_{-N+1}$.

(3) Generate a random time τ_2 with an exponential distribution with parameter Λ. Set $X(t) = \xi_1$ for $t \in [\tau_1, \tau_1 + \tau_2)$.

(4) Iterate. X is piecewise constant, takes values in S^δ, and has random jumps at times $\sum_{i=1}^{j} \tau_i$, $j \geqslant 1$.

APPENDIX B: DESCRIPTION OF THE PDMP

We give details on the definition of the PDMP modeling dry friction.

The process X defined in Sec. III A is a jump Markov process with the generator $Q^\delta f(x) = 2\tau^{-2}\delta^{-2}[\alpha_x f(x+\delta) - f(x) + (1-\alpha_x) f(x-\delta)]$, where $\alpha_x = \frac{1}{2}(1 - \frac{\tau\delta x}{2})$ if $|x| < x_N$, 0 if $x = x_N$, and 1 if $x = x_{-N}$. Here we assume $\tau\delta L_X^\delta < 2$ to guarantee that $\forall x \in S^\delta$, $\alpha_x \in [0, 1]$.

We introduce

$$B(x, y, v) = \begin{cases} \Delta + \mathfrak{b}(v) + \sqrt{\Gamma}x, & \text{if } y = -1, \\ 0, & \text{if } y = 0, \\ -\Delta + \mathfrak{b}(v) + \sqrt{\Gamma}x, & \text{if } y = 1. \end{cases} \tag{B1}$$

We define the state space

$$E = \bigcup_{(x,y)\in\mathbb{S}^\delta} E_{x,y}, \quad E_{x,y} = \{(x, y)\} \times H_{x,y}, \tag{B2}$$

where $\mathbb{S}^\delta = \{x_{-N}, \ldots, x_{k_- - 1}\} \times \{-1, 1\} \cup \{x_{k_-}, \ldots, x_{k_+}\} \times \{-1, 0, 1\} \cup \{x_{k_+ + 1}, \ldots, x_N\} \times \{-1, 1\}$, $H_{x,y} = (-\infty, 0)$ if $(x, y) \in \{x_{k-}, \ldots, x_N\} \times \{-1\}$, $H_{x,y} = (0, +\infty)$ if $(x, y) \in \{x_{-N}, \ldots, x_{k_+}\} \times \{1\}$, and $H_{x,y} = \mathbb{R}$ otherwise.

We can formulate the dynamics of Z starting from a state $z_0 = (x, y, z) \in E$ as follows:

(1) Generate a random time $T_1 = \min[\tau_1, T^\star(z_0)]$, where τ_1 is a random time with an exponential distribution with parameter $\Lambda = 2\tau^{-2}\delta^{-2}$, $T^\star(z_0) = \inf\{t \geqslant 0,\ \phi_{x,y}(t, v) = 0\}$ (with the convention $\inf \emptyset = +\infty$), and $\phi_{x,y}(t, v)$ is the flow

solution of

$$\partial_t \phi_{x,y}(t,v) = B(x,y,\phi_{x,y}(t,v)), \quad t>0,$$
$$\phi_{x,y}(0,v) = v. \tag{B3}$$

Then define $v_1 = \phi_{x_0,y_0}(T_1,v_0)$ and generate a random state $z_1=(x_1,y_1,v_1)$ from (x_0,y_0,v_1) using the probability transition matrix $\mathcal{Q}_{v_1}(x_1,v_1;x_0,v_0)$ (note that the velocity V does not jump during this transition):

$$\forall y\in\{-1,1\},\ \forall x\in\{x_{-N},\dots,x_{k_--1}\},$$
$$\mathcal{Q}_0(x,-1;x,y)=1, \tag{B4a}$$
$$\forall y\in\{-1,1\},\ \forall x\in\{x_{k_++1},\dots,x_N\},$$
$$\mathcal{Q}_0(x,1;x,y)=1, \tag{B4b}$$
$$\forall y\in\{-1,1\},\ \forall x\in\{x_{k_-},\dots,x_{k_+}\},$$
$$\mathcal{Q}_0(x,0;x,y)=1, \tag{B4c}$$
$$\forall x\in\{x_{k_-+1},\dots,x_{k_+-1}\},$$
$$\mathcal{Q}_0(x+\delta,0;x,0)=\alpha_x, \tag{B4d}$$
$$\forall x\in\{x_{k_-+1},\dots,x_{k_+-1}\},$$
$$\mathcal{Q}_0(x-\delta,0;x,0)=1-\alpha_x, \tag{B4e}$$
$$\mathcal{Q}_0(x_{k_-+1},0;x_{k_-},0)=\alpha_{x_{k_-}}, \tag{B4f}$$
$$\mathcal{Q}_0(x_{k_+-1},0;x_{k_+},0)=1-\alpha_{x_{k_+}}, \tag{B4g}$$
$$\mathcal{Q}_0(x_{k_--1},-1;x_{k_-},0)=1-\alpha_{x_{k_-}}, \tag{B4h}$$
$$\mathcal{Q}_0(x_{k_++1},1;x_{k_+},0)=\alpha_{x_{k_+}}, \tag{B4i}$$
$$\forall (x,y,v)\in E,\ v\neq 0,$$
$$\mathcal{Q}_v(x+\delta,y;x,y)=\alpha_x, \tag{B4j}$$
$$\forall (x,y,v)\in E,\ v\neq 0,$$
$$\mathcal{Q}_v(x-\delta,y;x,y)=1-\alpha_x. \tag{B4k}$$

The trajectory of Z for $t\in[0,T_1]$ is given by

$$Z_t=\begin{cases}(x_0,y_0,\phi_{x_0,y_0}(t,v_0)), & \text{if } 0\leqslant t<T_1\\ (x_1,y_1,v_1), & \text{if } t=T_1.\end{cases} \tag{B5}$$

When $\mathfrak{b}(v)=-v/\tau_L+\bar\gamma$ with $\tau_L\in(0,\infty)$, $\bar\gamma\in\mathbb{R}$ and due to the structure of B, explicit formula for $\phi_{x,y}(t,v)$ and $T^\star(z)$ are available. Straightforward calculations give

$$\phi_{x,y}(t,v)=|y|[e^{-t/\tau_L}(v-c(x,y))+c(x,y)],$$
$$c(x,y)=\tau_L(\bar\gamma+\sqrt{\Gamma}x-y\Delta),$$

and, using the notation $\Xi=\{(x,y,v)\in E, v>0 \text{ and } x<x_{k_+} \text{ or } v<0 \text{ and } x>x_{k_-}\}$,

$$T^\star(z)=\begin{cases}\tau_L\log\left(1-\frac{v}{c(x,y)}\right), & \text{if } (x,y,v)\in\Xi,\\ \infty, & \text{otherwise.}\end{cases}$$

Furthermore, the corresponding displacement on $[0,T_1]$ is $U(T_1)=\int_0^{T_1}\phi_{x_0,y_0}(t,v_0)dt=|y_0|[c(x_0,y_0)T_1+\tau_L(v_0-c(x_0,y_0))(1-e^{-T_1/\tau_L})]$.

(2) We can now define Z after T_1. Starting from $Z_{T_1}=z_1$, we generate the next jump time $T_2=T_1+\min(\tau_2,T^\star(z_1))$, where τ_2 is a random time with an exponential distribution with parameter Λ. Define $v_2=\phi_{x_1,y_1}(T_2-T_1,v_1)$ and the post-jump location $z_2=(x_2,y_2,v_2)$ from (x_1,y_1,v_2) using the probability transition matrix $\mathcal{Q}$. The trajectory of Z for $t\in[T_1,T_2]$ is given by

$$Z_t=\begin{cases}(x_1,y_1,\phi_{x_1,y_1}(t,v_1)), & \text{if } T_1\leqslant t<T_2,\\ (x_2,y_2,v_2), & \text{if } t=T_2.\end{cases} \tag{B6}$$

When $\mathfrak{b}(v)=-v/\tau_L+\bar\gamma$ with $\tau_L\in(0,\infty)$, $\bar\gamma\in\mathbb{R}$, the increment of displacement on $[T_1,T_2]$ is $U(T_2)-U(T_1)=|y_1|[c(x_1,y_1)(T_2-T_1)+\tau_L(v_1-c(x_1,y_1))(1-e^{-(T_2-T_1)/\tau_L})]$.

(3) Iterate. Z is piecewise deterministic and has random jumps at times T_j, $j\geqslant 1$.

APPENDIX C: A TECHNICAL PROOF

In order to prove that R_t converges in probability to zero as $t\to+\infty$, we proceed as follows. We can expand

$$R_t=\frac{1}{\sqrt{j_t}}\sum_{j=j_t}^{J_t-1}\mathcal{X}_j+\tilde{\mathcal{X}}_t, \quad \text{with } \tilde{\mathcal{X}}_t=\frac{1}{\sqrt{j_t}}\int_{t_{j_t}}^{t}V(s)ds.$$

The variable $\tilde{\mathcal{X}}_t$ goes to zero in probability as $t\to+\infty$ since $\mathbb{E}_{s_+}[|\tilde{\mathcal{X}}_t|]\leqslant j_t^{-1/2}\mathbb{E}_{s_+}[\int_0^{t_1}|V(s)|ds]=O(t^{-1/2})$. By introducing $Y_j=\sum_{j'=j\lfloor t^{1/4}\rfloor}^{(j+1)\lfloor t^{1/4}\rfloor-1}\mathcal{X}_{j_t+j'}$:

$$\left|\frac{1}{\sqrt{j_t}}\sum_{j=j_t}^{J_t-1}\mathcal{X}_j\right|\leqslant\frac{1}{\sqrt{j_t}}\sum_{j=-N_t}^{N_t}|Y_j|+O(t^{-1/4}),$$

with $N_t=|J_t-j_t|/\lfloor t^{1/4}\rfloor$. We have $N_t\leqslant\tilde N_t:=t^{1/4+1/16}$ with probability that goes to 1 as $t\to+\infty$, because $J_t-j_t=O(t^{1/2})$; therefore, for any $\epsilon>0$, for t large enough,

$$\mathbb{P}\left(\left|\frac{1}{\sqrt{j_t}}\sum_{j=j_t}^{J_t-1}\mathcal{X}_j\right|\geqslant\epsilon\right)$$
$$\leqslant\mathbb{P}(N_t\geqslant\tilde N_t)+\mathbb{P}\left(\frac{1}{\sqrt{j_t}}\sum_{j=-\tilde N_t}^{\tilde N_t}|Y_j|\geqslant\epsilon/2\right).$$

The variables Y_j are zero mean, independent, and identically distributed, with $\mathbb{E}_{s_+}[|Y_1|]\leqslant\mathbb{E}_{s_+}[Y_1^2]^{1/2}=t^{1/8}\mathbb{E}_{s_+}[\mathcal{X}_1^2]^{1/2}$. We then get by Markov inequality that

$$\mathbb{P}\left(\left|\frac{1}{\sqrt{j_t}}\sum_{j=j_t}^{J_t-1}\mathcal{X}_j\right|\geqslant\epsilon\right)$$
$$\leqslant\mathbb{P}(N_t\geqslant\tilde N_t)+\frac{\frac{2}{\sqrt{j_t}}\sum_{j=-\tilde N_t}^{\tilde N_t}\mathbb{E}_{s_+}[|Y_j|]}{\epsilon}$$
$$\leqslant\mathbb{P}(N_t\geqslant\tilde N_t)+\frac{Ct^{-1/16}}{\epsilon},$$

which shows the desired result:

$$\mathbb{P}(|R_t|\geqslant\epsilon)\overset{t\to+\infty}{\longrightarrow}0.$$

APPENDIX D: ASYMPTOTIC CONFIDENCE INTERVALS

In this Appendix we show how to build a confidence interval for D defined by (9) from the sample $\{(U_{\rm le}^{(k)},t_{\rm le}^{(k)})\}_{k=1}^N$. We

remark that

$$D = \Psi(\mathbb{E}_{s_+}[\boldsymbol{X}]),$$

with $\boldsymbol{X} = (X_j)_{j=1}^3$, $X_1 = U_{\rm le} = U(t_1)$, $X_2 = {U_{\rm le}}^2 = U(t_1)^2$, $X_3 = t_{\rm le} = t_1$, $\Psi(\boldsymbol{x}) = \frac{x_2 - x_1^2}{x_3}$. We define

$$\hat{\boldsymbol{S}}_N = \frac{1}{N}\sum_{k=1}^{N} \boldsymbol{X}^{(k)},$$

with $\boldsymbol{X}^{(k)} = (X_j^{(k)})_{j=1}^3$, $X_1^{(k)} = U_{\rm le}^{(k)}$, $X_2^{(k)} = {U_{\rm le}^{(k)}}^2$, $X_3^{(k)} = t_{\rm le}^{(k)}$. We have $\hat{D}_N = \Psi(\hat{\boldsymbol{S}}_N)$. Since the $\boldsymbol{X}^{(k)}$, $k = 1, \ldots, N$ are independent and identically distributed, we can apply the delta method [20, p. 79] and we get that the estimator $\hat{D}_N$ converges in distribution:

$$\sqrt{N}(\hat{D}_N - D) \overset{N\to+\infty}{\longrightarrow} \mathcal{N}(0, \sigma^2),$$

with $\sigma^2 = \nabla\Psi(\boldsymbol{S})^T \mathbf{C} \nabla\Psi(\boldsymbol{S})$, $\boldsymbol{S} = \mathbb{E}_{s_+}[\boldsymbol{X}]$, $\mathbf{C} = (C_{jl})_{j,l=1}^3$, $C_{jl} = \mathbb{E}_{s_+}[X_j X_l] - \mathbb{E}_{s_+}[X_j]\mathbb{E}_{s_+}[X_l]$. Here $\mathcal{N}(0, \sigma^2)$ stands for the normal distribution with mean 0 and variance σ^2. Denoting

$$\hat{C}_{N,jl} = \frac{1}{N}\sum_{k=1}^{N} X_j^{(k)} X_l^{(k)} - \hat{S}_{N,j}\hat{S}_{N,l},$$

the estimator

$$\hat{\sigma}_N^2 = \nabla\Psi(\hat{\boldsymbol{S}}_N)^T \hat{\mathbf{C}}_N \nabla\Psi(\hat{\boldsymbol{S}}_N)$$

converges to σ^2 in probability. By Slutsky's theorem we get that

$$\sqrt{N}\hat{\sigma}_N^{-1}(\hat{D}_N - D) \overset{N\to+\infty}{\longrightarrow} \mathcal{N}(0, 1)$$

in distribution. This gives that the interval

$$(\hat{a}_N, \hat{b}_N) = \left(\hat{D}_N - q_{1-\alpha/2}\frac{\hat{\sigma}_N}{\sqrt{N}}, \hat{D}_N + q_{1-\alpha/2}\frac{\hat{\sigma}_N}{\sqrt{N}}\right),$$

with $q_{1-\alpha/2}$ the $(1-\alpha/2)$ quantile of the distribution $\mathcal{N}(0, 1)$, with a confidence interval of asymptotic level $1-\alpha$:

$$\lim_{N\to+\infty} \mathbb{P}(D \in (\hat{a}_N, \hat{b}_N)) = 1 - \alpha.$$

APPENDIX E: ALGORITHMS RELATED TO THE PDMP

In this Appendix we give the details of the function's interjump(X, Y, V), displacement (X, Y, V), flow $(X, Y, V, \delta T)$, and jump $(X, Y; V)$ for PDMP simulation. The formulas are valid when $\mathfrak{b}(v) = -v/\tau_L + \bar{\gamma}$ with $\tau_L \in (0, \infty)$, $\bar{\gamma} \in \mathbb{R}$.

Algorithm 4. Simulation of an interjump time from (X, Y, V).

Result: $\delta T = \text{interjump}(X, Y, V)$
$u = \text{uniform}()$;
$\delta T = \min(-\frac{\log(u)}{\Lambda}, T^\star(X, Y, V))$.

Algorithm 5. Formula for the increment of displacement from (X, Y, V) on the time interval $[T, T + \delta T]$.

Result: $\delta U = \text{displacement}(X, Y, V, T, T + \delta T)$
$\delta U = |Y|[c(X, Y)\delta T + \tau_L(V - c(X, Y))(1 - e^{-\delta T/\tau_L})]$;

Algorithm 6. Formula for the flow from (X, Y, V) on the time interval $[T, T + \delta T]$.

Result: $\hat{V} = \text{flow}(X, Y, V, \delta T)$
$c(X, Y) = \tau_L(\bar{\gamma} + \sqrt{\Gamma}X - Y\Delta)$;
$\hat{V} = |Y|[e^{-\delta T/\tau_L}(v - c(X, Y)) + c(X, Y)]$;

Algorithm 7. Simulation of a jump from (X, Y, V).

Result: $(X', Y', V) = \text{jump}(X, Y; V)$
$\alpha = \frac{1}{2}(1 - \frac{\tau\delta X}{2})\mathbf{1}_{\{|X|<L_X^\delta\}} + (1 - X^{-1}\max(X, 0))\mathbf{1}_{\{|X|=L_X^\delta\}}$;
$A = (|Y| = 1)$ and $(V = 0)$;
$B = (Y = 0)$ and $(V = 0)$ and $((X = x_{k_-})$ or $(X = x_{k_+}))$;
if A **then**
  $Y' = -\mathbf{1}_{\{X\leqslant x_{k_- -1}\}}\mathbf{1}_{\{Y=1\}} + \mathbf{1}_{\{X\geqslant x_{k_+ +1}\}}\mathbf{1}_{\{Y=-1\}}$
else
  u= uniform()
  $X' = (X + \delta)\mathbf{1}_{\{u\leqslant\alpha\}} + (X - \delta)\mathbf{1}_{\{u>\alpha\}}$;
  if B **then**
    $Y' = \mathbf{1}_{\{X=x_{k_+}\}}\mathbf{1}_{\{u\leqslant\alpha\}} - \mathbf{1}_{\{X=x_{k_-}\}}\mathbf{1}_{\{u>\alpha\}}$;
  end
end

[1] F. P. Bowden and D. Tabor, *Friction and Lubrication of Solids* (Oxford University Press, Oxford, 2001).

[2] B. N. J. Persson, *Sliding Friction: Physical Principles and Applications* (Springer, Berlin, 1998).

[3] P.-G. de Gennes, Brownian motion with dry friction, J. Stat. Phys. **119**, 953 (2005).

[4] H. Touchette, T. Prellberg, and W. Just, Exact power spectra of Brownian motion with solid friction, J. Phys. A: Math. Theor. **45**, 395002 (2012).

[5] H. Touchette, E. Van der Straeten, and W. Just, Brownian motion with dry friction: Fokker-Planck approach, J. Phys. A: Math. Theor. **43**, 445002 (2010).

[6] Y. Chen and W. Just, First-passage time of Brownian motion with dry friction, Phys. Rev. E **89**, 022103 (2014).
[7] Y. Chen and W. Just, Large-deviation properties of Brownian motion with dry friction, Phys. Rev. E **90**, 042102 (2014).
[8] T. Feghhi, W. Tichy, and A. W. C. Lau, Pulling a harmonically bound particle subjected to Coulombic friction: A nonequilibrium analysis, Phys. Rev. E **106**, 024407 (2022).
[9] P. C. Bressloff, Stochastic resetting and the mean-field dynamics of focal adhesions, Phys. Rev. E **102**, 022134 (2020).
[10] P. S. De and R. De, Stick-slip dynamics of migrating cells on viscoelastic substrates, Phys. Rev. E **100**, 012409 (2019).
[11] P. M. Geffert and W. Just, Nonequilibrium dynamics of a pure dry friction model subjected to colored noise, Phys. Rev. E **95**, 062111 (2017).
[12] T. K. Caughey and J. K. Dienes, Analysis of a nonlinear first-order system with white noise input, J. Appl. Phys. **32**, 2476 (1961).
[13] P. S. Goohpattader, S. Mettu, and M. K. Chaudhury, Experimental investigation of the drift and diffusion of small objects on a surface subjected to a bias and an external white noise: Roles of Coulombic friction and hysteresis, Langmuir **25**, 9969 (2009).
[14] J. Garnier, Z. Lu, and L. Mertz, A piecewise deterministic Markov process approach modeling a dry friction problem with noise, SIAM J. Appl. Math. **83**, 1392 (2023).
[15] M. H. A. Davis, Piecewise-deterministic Markov processes: A general class of nondiffusion stochastic models, J. Roy. Statist. Soc. Ser. B **46**, 353 (1984).
[16] B. De Saporta, F. Dufour, and H. Zhang, Numerical methods for simulation and optimization of piecewise deterministic Markov processes: Application to reliability (Wiley, Hoboken, NJ, 2015).
[17] E. Pardoux and A. Răşcanu, *Stochastic Differential Equations, Backward SDEs, Partial Differential Equations* (Springer International, Cham, 2014).
[18] H. Brézis, Opérateurs maximaux monotones et semi-groupes de contractions dans les espaces de Hilbert, North-Holland, Amsterdam, London, North-Holland Mathematics Studies, No. 5. Notas de Matemaíca (50) (American Elsevier, New York, 1973).
[19] H. Hayakawa, Langevin equation with Coulomb friction, Physica D **205**, 48 (2005).
[20] L. Wasserman, *All of Statistics: A Concise Course in Statistical Inference* (Springer, New York, 2004).